AIP | Physics of Plasmas

On the accuracy and reliability of different fluid models of the direct current glow discharge

I. Rafatov, E. A. Bogdanov, and A. A. Kudryavtsev

Citation: Phys. Plasmas 19, 033502 (2012); doi: 10.1063/1.3688875
View online: http://dx.doi.org/10.1063/1.3688875
View Table of Contents: http://pop.aip.org/resource/1/PHPAEN/v19/i3
Published by the American Institute of Physics.

On the accuracy and reliability of different fluid models of the direct current glow discharge

I. Rafatov,[1,a)] E. A. Bogdanov,[2] and A. A. Kudryavtsev[2]
[1]*Physics Department, Middle East Technical University, Ankara, Turkey*
[2]*Saint Petersburg State University, St. Peresburg, Russia*

(Received 14 November 2011; accepted 26 January 2012; published online 5 March 2012)

We developed and tested 2D "extended fluid model" of a dc glow discharge using COMSOL MULTIPHYSICS software and implemented two different approaches. First, assembling the model from COMSOL's general form pde's and, second, using COMSOL's built-in Plasma Module. The discharge models are based on the fluid description of ions and excited neutral species and use drift-diffusion approximation for the particle fluxes. The electron transport as well as the rates of electron-induced plasma-chemical reactions are calculated using the Boltzmann equation for the EEDF and corresponding collision cross-sections. The self-consistent electric field is calculated from the Poisson equation. Basic discharge plasma properties such as current-voltage characteristics and electron and ion spatial density distributions as well as electron temperature and electric field profiles were studied. While the solutions obtained by two different COMSOL models are essentially identical, the discrepancy between COMSOL and CFD-ACE+ model solutions is about several percents and caused by the difference in the models due to undocumented details in the software packages. We also studied spatial distributions of particle fluxes in discharge plasma and identified the existence of vortex component of the discharge current. © *2012 American Institute of Physics*. [http://dx.doi.org/10.1063/1.3688875]

I. INTRODUCTION

Glow discharges are of topical interest for lots of technological applications like plasma light sources, plasma processing for surface modification, and plasma chemistry.[1] Therefore, a detailed understanding of the fundamental processes of glow discharges is required for the design, characterization, and optimization of the discharge parameters in these plasma applications. One of the ways to gain such understanding is to model the processes occurring in the plasma.

The modelling approaches can be classified as fluid methods, kinetic (particle) methods and their combinations, called hybrid methods, which represent a compromise between the computationally very efficient fluid models and fully kinetic particle models that require very extensive computations.

The reliability of any model is determined by its bottleneck, i.e., by the least accurately known element. Such an element in fluid models of glow discharges is the treatment of electron dynamics, because in most cases, electrons in these plasmas are far from equilibrium (electron transport in dc glow discharges is highly nonlocal[2,3]). Exact description of the motion of electrons in gas discharges can be obtained by the numerical solution of the electron Boltzmann equation.[4–7] Hybrid models, in which slow plasma species are treated within the frame of the fluid model, while fast species (in particular, fast electrons, using Monte Carlo simulations) are treated as particles, provide another way to improve the drawbacks of fluid model.[8–13]

In fluid models of glow discharges, all the plasma species, including electrons, are treated as continuum. These models involve, for all plasma species, the continuity equation, momentum equation, and energy equation (usually only for electrons), which are velocity moments of the kinetic Boltzmann equation. The system is completed by the Poisson equation for the self-consistent electric field. Each of the fluid equations contain transport and rate coefficients, which represent the effect of collisions and which are input data for the fluid model.[1,14] In fluid models of glow discharge, momentum equations are usually reduced to the drift-diffusion equation and "local field approximation" (LFA) for transport and rate coefficients is employed. This means that the particle transport (mobility and diffusion) coefficients as well as the particle volume sources are defined as functions of the local value of the reduced electric field E/p (where E is the magnitude of the field and p is the background gas pressure), which, in general, is an unacceptable approximation. One of the reasons is that since the ionization rate in the case of LFA is a function of the local electric field strength, ionization could occur in the cathode sheath only, where the electric field is strong enough and could not occur in the negative glow and Faraday dark space where the electric field is weak. However, it is known that bright luminous regions of high charge density in the negative glow are produced by nonlocal ionization and excitation from fast electrons entering the negative glow from the cathode sheath (see, e.g., Refs. 2, 3, and 15). Due to this nonlocal ionization, the ions which cause the secondary emission of electrons from the cathode come not only from the cathode sheath but also from regions of the plasma with a weak electric field.

In order to remedy the disadvantages associated with the LFA and incorporate to a certain extent, the nonlocal transport of electrons into fluid models, an approach ("extended

[a)]Electronic mail: rafatov@metu.edu.tr.

fluid model," which is also known as "local mean energy approximation," LMEA, as opposed to LFA) was suggested in Ref. 15 that is used in this work (its different modifications were applied in Refs. 11, 16–22). The idea behind this approach is that in the calculation of the electron transport (mobility and diffusion) coefficients as well as the kinetic coefficients (electron-impact reaction rates for excitation and ionization processes), by solving the kinetic Boltzmann equation, as functions of electron temperature T_e rather than local value of the electric field. Spatial distribution of the electron temperature, T_e, within this model is obtained from the solution of the energy balance equation for electrons, which along with the volume processes takes also account of transfer by heat conduction. In this case, electron heating source in the plasma becomes nonlocal, because the effect of heating caused by the heat flux from the cathode layer, where main Joule heating occurs, is taken into account properly.

In this work, we developed and tested the 2D (axial-symmetric) "extended fluid model," using the COMSOL MULTIPHYSICS software.[23] More exactly, we implemented two modelling approaches. First, we constructed the model using "general form" COMSOL pde's, and second, employing COMSOL's built in Plasma Module. For validation of the numerical models, we followed the discharge conditions in Ref. 16 (low pressure argon gas) and plasma-chemical model in Ref. 20 and showed, first, that the developed COMSOL models lead to the identical results and, second, that these results agree sufficiently well with those obtained from the CFD-ACE+ solver,[24] subject to the same discharge conditions and identical particle transport and plasma-chemistry (the same set of reaction and corresponding cross-sections).

Analysis of the calculation results showed that the model describes adequately the basic properties of the glow discharge, reproduces correctly current-voltage characteristics (CVC) and specific discharge modes occurring along the CVC (including normal mode and such a 2D effect as formation of a normal current density) as well as the two-dimensional spatial profiles of the discharge parameters (such as the charged particle densities, temperature, and the electric potential and field).

We also studied the particle flux spatial distributions in the case of short and longer glow discharges. In analogy with the previously reported results,[25] where a presence of vortex component of electron fluxes have been identified in the case of ICP discharge (that means that the electron and ion fluxes do not satisfy the conventionally adopted ambipolarity condition), we have shown the presence of vortex currents also in glow discharge plasma, for a short discharge, and vanishing of it in the positive column of longer glow discharge.

The paper is organized as follows. Section II introduces the model of the glow discharge. There we describe the equations of the model, the boundary conditions imposed, and details of calculation of the particle transport as well as the source terms in the particle and energy balance equations. Calculation results are discussed in Sec. III. This section also includes comparison of different "extended fluid models" as well as comparison between 1D and 2D model solutions. Section IV deals with the analysis of particle fluxes in the plasma. Finally, Sec. V contains the conclusions.

II. MODEL

In this section, we describe the glow discharge model implemented in the work. Equations of the model and boundary conditions are given. Treatment of transport in plasma and account of particle creation and destruction in volume processes are described.

A. Equations

The gas-discharge model includes continuity equations for the charged and excited particles,

$$\frac{\partial n_k}{\partial t} + \nabla \cdot \mathbf{\Gamma}_k = S_k, \tag{1}$$

where particle flux $\mathbf{\Gamma}$ is in the drift-diffusion approximation,

$$\mathbf{\Gamma}_k = sgn(q_k) n_k \mu_k \mathbf{E} - D_k \nabla n_k \tag{2}$$

(see, e.g., Ref. 1). Electric field is obtained from solution of the Poisson's equation in the electrostatic approximation,

$$\epsilon_0 \nabla \cdot \mathbf{E} = \sum_k q_k n_k, \quad \mathbf{E} = -\nabla \phi. \tag{3}$$

In these equations, subscripts k indicate the kth species. We will also use subscripts i, e, m, and g for ions, electrons, metastable atoms, and background gas, respectively. $\mathbf{E}$ and ϕ are the electric field and potential, q is the charge, ϵ_0 is the dielectric constant, μ and D are the particle mobility and diffusion coefficients, and S is the particle creation rate.

Equations (1)–(3), with particle transport coefficients and volume source terms in the particle balance equations specified, form the traditional "simple fluid" model. Within this model, mobility and diffusion coefficients as well as the particle creation rates, in general, are defined as functions of the reduced electric field E/p ("local field approximation") or approximated by constants, usually for electron transport coefficients μ_e and D_e. Einstein relation between mobility and diffusion, $D/\mu = k_B T/e$, is assumed to be valid. Here, p denotes the gas pressure, T the kinetic temperature, and k_B the Boltzmann constant. In order to incorporate the nonlocal transport of electrons into the fluid model, electron energy equation is included in the set of "extended fluid model" equations (see, e.g., Refs. 1 and 18),

$$\frac{\partial n_\varepsilon}{\partial t} + \nabla \cdot \mathbf{\Gamma}_\varepsilon = -e\mathbf{\Gamma}_e \cdot \mathbf{E} - \frac{3}{2}\frac{m_e}{m_g}\nu_{ea} n_e k_B (T_e - T_g) - \sum_j \Delta E_j R_j, \tag{4}$$

where $n_\varepsilon = n_e \bar{\varepsilon}$ is the electron energy density, $\bar{\varepsilon} = 3/2 k_B T_e$ denotes the mean electron energy, and density of the electron energy flux is

$$\mathbf{\Gamma}_\varepsilon = -D_\varepsilon \nabla n_\varepsilon - \mu_\varepsilon \mathbf{E} n_\varepsilon. \tag{5}$$

In the source term of Eq. (4), the first term describes the Joule heating (or cooling) of electrons in the electric field, second term, with ν_{ea} denoting the electron-atomic elastic collision frequency describes the elastic loss, and the last

TABLE I. Elementary reactions considered in this study. Label Boltz indicates that constant was calculated from local Boltzmann equation.

Index	Reaction	Type	$\Delta E(eV)$	Constant
1	$e + Ar \rightarrow e + Ar$	Elastic collision	0	Boltz.
2	$e + Ar \rightarrow 2e + Ar^+$	Direct ionization	15.8	Boltz.
3	$e + Ar \leftrightarrow e + Ar^*$	Excitation	11.4	Boltz.
4	$e + Ar \rightarrow e + Ar$	Excitation	13.1	Boltz.
5	$e + Ar^* \rightarrow 2e + Ar^+$	Stepwise ionization	4.4	Boltz.
6	$2Ar^* \rightarrow e + Ar^+ + Ar$	Penning ionization	–	$6.2 \times 10^{-10}\,\mathrm{cm^3\,s^{-1}}$
7	$Ar^* \rightarrow h\nu + Ar$	Radiation (including trapping)	–	$1.0 \times 10^{7}\,\mathrm{s^{-1}}$

term describes the energy loss in inelastic collisions. ΔE_j and R_j are the energy loss (or gain) due to inelastic collision and corresponding reaction rate, m is the particle mass, background gas temperature $T_g = 300\,\mathrm{K}$.

B. Transport coefficients

The plasma-chemical model in this work is identical to the model in Refs. 16 and 20. Calculations are performed for a argon gas, and three plasma species, namely, electrons, positive ions, and metastable atoms, are taken into account. The set of reactions is given in Table II, and collision cross-sections are shown in Fig. 1. The first process in Table I is an elastic scattering of electrons. The cross-section for this process is used to calculate the effective frequency ν_{ea}, mobility, μ_e, and diffusion, D_e,

$$\mu_e = -\frac{1}{n_e}\frac{e}{m_e}\int_0^\infty D_r\sqrt{\varepsilon}\frac{\partial}{\partial\varepsilon}f_0(\varepsilon)d\varepsilon, \tag{6}$$

$$D_e = \frac{1}{n_e}\int_0^\infty D_r\sqrt{\varepsilon}f_0(\varepsilon)d\varepsilon, \tag{7}$$

where $\varepsilon = mv^2/2e$ is the electron kinetic energy (in eV units), and $D_r = 2\varepsilon/3m_e\nu_{ea}$ is the space diffusion coefficient, $f_0(\varepsilon)$ is the EEDF obtained from the solution of local Boltzmann equation, and which is normalized by the expression

$$\int_0^\infty f_0(\varepsilon)\sqrt{\varepsilon}d\varepsilon = 1. \tag{8}$$

Heavy particle energies are assumed to follow Maxwell distribution functions. Their mobility and diffusion coefficients

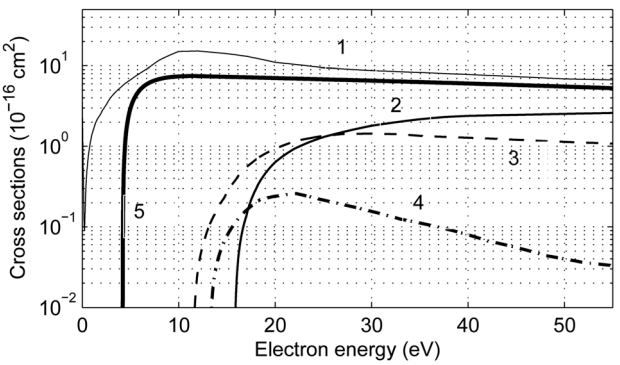

FIG. 1. Electron cross sections for (1) elastic, (2) direct ionization, (3) excitation, (4) excitation, and (5) stepwise ionization collisions in argon, used in the model. Curve labels correspond to indices of corresponding processes in Table I.

are approximated by constant parameters, which depend on a background gas density. Moreover, ion mobility and diffusion are related by the expression $D_i/\mu_i = k_B T_i/e$ with $T_i = T_g$.

Energy transport coefficients in Eq. (5) are related to particle transport coefficients via $\mu_\varepsilon = (5/3)\mu_e$ and $D_\varepsilon = (5/3)D_e$.[18] In the literature, in order to identify the term containing heat conductivity, electron energy flux $\mathbf{\Gamma}_\varepsilon$ (5) is also presented in the form

$$\mathbf{\Gamma}_\varepsilon = \frac{5}{2}k_B T_e\mathbf{\Gamma}_e - \lambda_e\nabla k_B T_e, \tag{9}$$

with $\lambda_e = \frac{5}{2}n_e D_e$.[16,18]

C. Source terms

Volume source terms S_k in the particle balance equations (1) are determined by the reactions occurring in the discharge,

$$S_k = \sum_i R_i - \sum_j R'_j, \tag{10}$$

where R_i and R'_j are the rates of corresponding reactions. These are proportional to the concentrations of the reacting components.

Electron balance in the model is determined by the direct, stepwise, and Penning ionization processes,

$$\begin{aligned} S_e &= S_i = R_2 + R_5 + R_6 \\ &= K_2 n_0 n_e + K_5 n_m n_e + K_6 n_m^2, \end{aligned} \tag{11}$$

where the rates for ions and electrons are identical due to the particle conservation. Here, R_2, R_5, and R_6 denote direct, stepwise, and Penning ionization reaction rates, K_2, K_5, and K_6 denote the constants of these reactions, and n_0 is concentration of neutral atoms. Indices of rates and constants here coincide with indices of processes in Table I.

Balance of excited atoms is determined by the reactions of excitation, stepwise ionization, Penning ionization, and radiation,

$$\begin{aligned} S_m &= R_3 - R_5 - 2R_6 - R_7 \\ &= K_3 n_0 n_e - K_5 n_m n_e - 2K_6 n_m^2 - K_7 n_m. \end{aligned} \tag{12}$$

Reaction rate constants K depend on the energy distribution of the related component. For reactions between heavy particles, which are assumed to be Maxwellian, rate constant

is obtained from Arrhenius's law. For electron-induced reactions (processes 1–5 in the Table I), rate constants of processes are calculated by convolving the EEDF, obtained from a solution of local Boltzmann kinetic equation, with the corresponding cross-sections,

$$K_R = \int_0^\infty \sigma_R(\varepsilon)\sqrt{\varepsilon} f_0(\varepsilon) d\varepsilon, \tag{13}$$

where dependence of collision cross sections σ_R of reaction R on energy ε is shown in the Fig. 1.

Separate solver for the electron Boltzmann equation has been used to produce the so called LUT's (look-up-tables) and thereby relate mean electron energy to the electron transport coefficients (diffusion, D_e, and mobility, μ_e) as well as the rates S of electron-induced plasma-chemical reactions for excitation and ionization. Although built-in "Boltzmann Equation" model is available in COMSOL 4.1, we used LUT's generated by CFD-ACE+ package. Incorporating the LUT's into the numerical model significantly saves processing time, because in this case, computationally expensive Boltzmann Module runs only once.

D. Boundary conditions

Boundary conditions for the positive ions and metastable atoms at the anode, cathode, and the wall of the discharge tube are given as follows (see, e.g., Refs. 15 and 26):

$$\hat{\mathbf{n}} \cdot \mathbf{\Gamma}_i = 1/4 v_i n_i + \alpha n_i \mu_i (\hat{\mathbf{n}} \cdot \mathbf{E}), \tag{14}$$

$$\hat{\mathbf{n}} \cdot \mathbf{\Gamma}_m = 1/4 v_m n_m. \tag{15}$$

Here, thermal velocity $v_j = \sqrt{8k_B T_j/\pi m_j}$ ($j = e, i, m$), particle flux density $\mathbf{\Gamma}$ is described by Eq. (2), $\hat{\mathbf{n}}$ is the normal unit vector pointing towards the surface, and α is a switching function (either 0 or 1) depending on positive ion drift direction at the surface: $\alpha = 1$ if $(\hat{\mathbf{n}} \cdot \mathbf{E}) > 0$ and $\alpha = 0$ otherwise.

Boundary conditions for the electron density and electron energy density at the anode and dielectric wall are

$$\hat{\mathbf{n}} \cdot \mathbf{\Gamma}_e = 1/4 v_e n_e, \tag{16}$$

$$\hat{\mathbf{n}} \cdot \mathbf{\Gamma}_\varepsilon = 1/3 v_e n_\varepsilon, \tag{17}$$

while at the cathode

$$\hat{\mathbf{n}} \cdot \mathbf{\Gamma}_e = 1/4 v_e n_e - \gamma \hat{\mathbf{n}} \cdot \mathbf{\Gamma}_i, \tag{18}$$

$$\hat{\mathbf{n}} \cdot \mathbf{\Gamma}_\varepsilon = 1/3 v_e n_\varepsilon - 2k_B T_e \gamma \hat{\mathbf{n}} \cdot \mathbf{\Gamma}_\mathbf{i}, \tag{19}$$

where γ is the secondary electron emission coefficient. Boundary conditions for the electron energy transport (17) and (19) are consistent with the boundary condition for electron transport (16) and (18), $\hat{\mathbf{n}} \cdot \mathbf{\Gamma}_\varepsilon = 2k_B T_e (\hat{\mathbf{n}} \cdot \mathbf{\Gamma}_e)$ and taken in the form Ref. 27 (p. 136).

We imposed the symmetry condition along the z-axis for all the variables, $\hat{\mathbf{n}} \cdot \mathbf{\Gamma}_j = 0$ ($j = i, e, m, n_\varepsilon$).

For the electric potential, we set $\phi = U_d$ at the anode, $\phi = 0$ at the cathode, while at the dielectric surface

$$\frac{\partial \phi}{\partial r} = \frac{1}{\epsilon_0}\sigma, \tag{20}$$

where the surface charge density σ is calculated from the equation

$$\frac{\partial \sigma}{\partial t} = \hat{\mathbf{n}} \cdot e(\mathbf{\Gamma}_i - \mathbf{\Gamma}_e). \tag{21}$$

III. MODELLING RESULTS

Let us now proceed to a discussion of the modelling results. These results include current-voltage characteristics (CVC) of the discharge and spatial distributions of the discharge parameters in the CVC points.

For modelling and numerical solutions, we used the finite element computational package COMSOL MULTIPHYSICS ™ (version 4.1).[23] Calculations have been carried out for argon gas. We looked for the steady-state solutions. Three chemical species (electrons (e), positive ions (Ar+), and metastable atoms Ar*)) and seven elementary reactions (direct ionization, electronic excitation from ground-state atoms, step-wise ionization from metastables, Penning ionization, and radiative de-excitation) are considered in the gas phase (see Table I). The cross sections of elementary processes are displayed in Fig. 1.

Figure 3 demonstrates the CVC curves for the discharge conditions and parameter regime Ref. 16 (namely, argon at pressure $p = 3$ torr, discharge gap $L = 1$ cm, discharge radius $R = 1.5$ cm, and secondary emission coefficient $\gamma = 0.1$). Basic parameters of the discharge for the seven points numbered along the CVC curve are listed in Table II, where I_d and U_d there denote the discharge current and voltage, d denotes the width of the cathode layer, and r^* denotes the radius of the cathode spot. The left down-tending branch of the CVC curve (points 1–3) corresponds to the subnormal discharge, the central part (points 3–5) corresponds to the normal, and the right up-tending branch (points 5–7) to the abnormal glow discharge. In the subnormal regime, voltage drops from 280 to 220 V, while current varies from 0.01 to 0.6 mA. For normal glow, voltage between the electrodes is essentially constant (about 220 V) over the current range from 0.6 mA to 10 mA. In abnormal regime, voltage grows from 220 to 300 V with currents ranging from 10 mA to 500 mA.

It should be noted that simulation of the discharge in the abnormal mode (which is stable) can be carried out without coupling the discharge model with the external circuit (see Fig. 2), just specifying the value of gap voltage U_d instead. However, when simulating the subnormal and normal discharges, the discharge equation (1)–(4) are completed with the equation for the external circuit,

TABLE II. Parameters of the glow discharge for the points 1–7 along the current-voltage curve in Fig. 3.

	U_d (V)	I_d (mA)	J_d (mAcm^{-2})	r^* (cm)	d (cm)
1	236	0.088	0.14	0.26	0.60
2	214	0.29	1.39	0.15	0.18
3	210	0.58	2.46	0.18	0.14
4	207	2.93	3.03	0.47	0.13
5	208	11.7	3.33	0.97	0.13
6	216	28.4	4.93	1.29	0.11
7	300	310	44.4	1.48	0.058

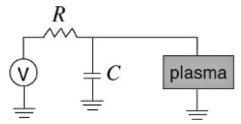

FIG. 2. RC circuit used in the model.

$$\frac{dU_d}{dt} + \frac{1}{\mathcal{C}}\left(I_d - \frac{U_{src} - U_d}{\mathcal{R}}\right) = 0, \qquad (22)$$

Otherwise, the solution will converge to the abnormal discharge, corresponding to the specified voltage U_d. In this equation, U_{src} is the applied dc voltage, $\mathcal{R}$ is the resistance of the circuit, and $\mathcal{C}$ is the external capacitance. Similarly to Ref. 16, we specified $\mathcal{C} = 1$ pF and $U_{src} = 500$ V and to describe the different discharge regimes displayed in Fig. 3, we varied value of the resistance $\mathcal{R}$ between 10 M Ω and 500 Ω.

In full agreement with experimental observations,[1] in the normal glow regime, cathode spot area expands continuously with increasing current, while current density on the cathode surface is keeping constant. This inherently two-dimensional characteristic of the discharge, which is, therefore, not realizable in the one-dimensional model, is demonstrated in the Fig. 3(b), where the current density J_d is plotted along the horizontal axis instead of the current magnitude I_d, and the points indicated along the CVC curves in the panels (a) and (b) correspond to the same regimes. Note that while the points 3, 4, and 5 in the first figure are isolated, which means that the current magnitude is different for these regimes, the same points in the panel (a) practically coincide, i.e., the current density for these points is nearly the same.

Let us now turn to the analysis of the results, corresponding to the three typical glow discharge regimes. We will consider spatial distributions of discharge plasma characteristics, corresponding to regimes indicated by the numbers 1, 4, and 7 in the Fig. 3 and Table II.

Point 1 corresponds to the subnormal regime. As can be seen from the charged particle (ion and electron) 2D density plots (Figs. 4(a) and 4(b)) and from the density axial profiles (Fig. 4(c)), quasineutrality in this regime does not hold. Since currents are weak and the electron mobility far exceeds that of ions, the ion density is greater than the electron density over the entire discharge volume.[1]

Density plots of charged particles for the point 4, which corresponds to the normal mode, are demonstrated in Fig. 5.

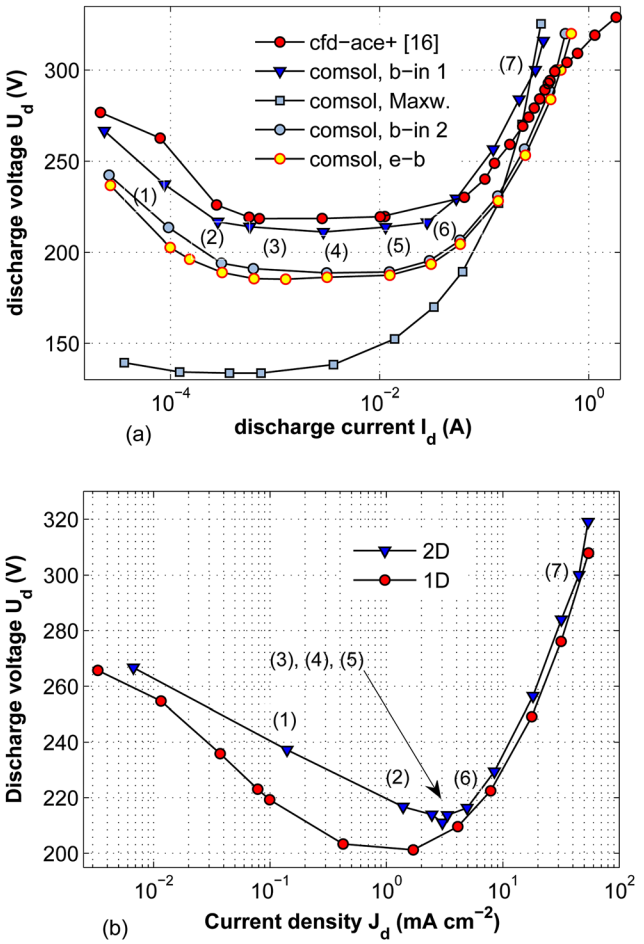

FIG. 3. (Color online) Current-voltage characteristics of discharges in argon at pressure $p = 3$ torr, discharge gap $L = 1$ cm, tube radius $R = 1.5$ cm, and $\gamma = 0.1$. (a) $U_d = U_d(I_d)$, (b) $U_d = U_d(J_d)$.

As is evident from these figures, quasineutrality is violated in the cathode layer only, whereas the remaining part of the discharge is the plasma with equal electron and ion number densities, $n_e \approx n_i$.

Finally, Fig. 6 shows 2D and axial density plots for the abnormal discharge (point 7). As can be seen from the density axial profiles, in this regime, the cathode layer tends to decrease in width, leaving the rest of discharge volume quasineutral, $n_e \approx n_i$.

As illustrated in Fig. 7(a), in the subnormal mode, electric field is weakly distorted, potential varies nearly linearly from the cathode to the anode. In normal and abnormal

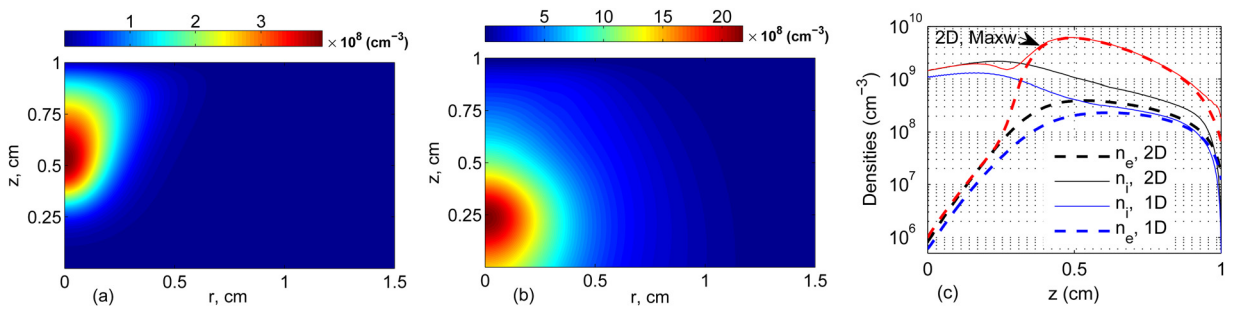

FIG. 4. (Color online) 2D density profiles of the electrons n_e (a) and ions n_i (b), and axial density profiles of the electrons and ions (c). 1D and 2D in panel (c) refer to one- and two-dimensional models, Maxw. indicates result with the Maxwellian EEDF. Parameter regime: point 1 in the Fig. 3 and Table II.

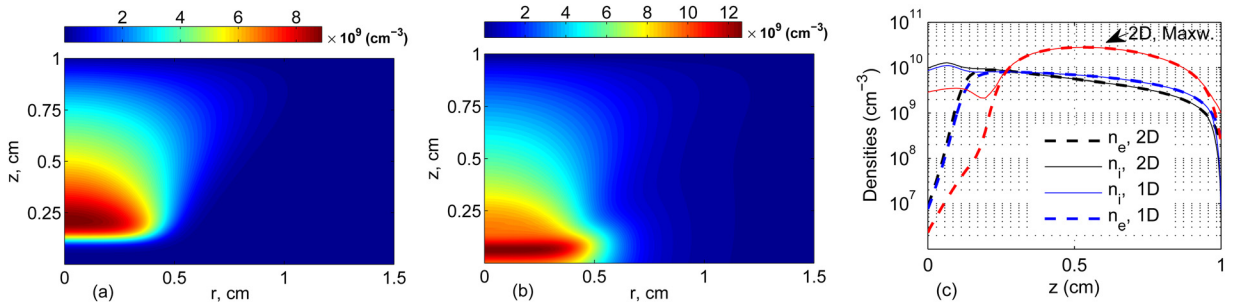

FIG. 5. (Color online) The same as in Fig. 4 but for the regime 4 in the Fig. 3 and Table II.

regimes, formation of a (positive) volume charge in the cathode vicinity leads to a significant growth of the electric potential within the cathode layer, while the remaining part of the discharge gap is filled with the plasma, where the electric field strength is relatively weaker. Change in the electron temperature is significant in the cathode layer of normal and abnormal discharge, and weak in the subnormal discharge (Fig. 7(b)).

Figures 8(a) and 8(b) demonstrate the cathode current density and cathode sheath thickness $d(r)$ radial profiles for the regimes 1–7 in the Figure 3 and Table II. The function d in Fig. 8(b) is the distance from the cathode satisfying the condition $n_e(r,d) = 0.5n_i(r,d)$. As can be seen from Fig. 8(a), model adequately describes one of the most fundamental and important two-dimensional properties of the gas discharge, namely, the cathode spot area expands and contradicts as current increases and decreases in the normal regime (Fig. 8(a)): discharge tends to occupy the entire cathode surface in the subnormal and abnormal modes, whereas in the normal mode it occupies only part of the cathode.

A. Comparison with different "extended fluid model" results

We used COMSOL MULTIPHYSICS^{TM} finite element computational software (version 4.1) (Ref. 23) for modelling and numerical solutions. Important advantage of COMSOL MULTIPHYSICS, compared to some other package programs, which do not allow much room for modifications of the predefined physics and underlying model equations, is its flexibility in specifying the model, modifying the predefined physics interfaces, etc. For instance, within the CFD-ACE+, the description of plasma chemistry involved (and consequently the source terms of balance equations in section II) is strongly limited to selection among the predefined processes only. COMSOL MULTIPHYSICS is more flexible in this sense.

More specifically, we implemented two modelling approaches. First, we developed a model, using "general form" COMSOL pde's for the discharge equations (1)–(4) and, second, employing COMSOL's "Plasma Module" with "DC Discharge" interface. In the first case, the process of derivation of the model is absolutely explicit and consists of specifying and assembling together all the model elements (which include the equations, boundary conditions, transport parameters, descriptions of plasmachemical reactions, etc.) "by hand." Therefore, it is meaningful to compare our "homemade" model with the model involving the built-in plasma module, for the same discharge size and shape (we used two-dimensional parallel-plane geometry with cylindrical symmetry), and identical transport parameters and set of plasma chemical reactions together with the corresponding collision cross sections.

CVC curves obtained by these models are indicated as "comsol, e-b" and "comsol, b-in" in the Fig. 3(a). All the CVC curves in Fig. 3(a) have been calculated subject to the boundary conditions as described in the Sec. III D, except for the curve "comsol, b-in 1," which, in an effort to demonstrate the effect of boundary conditions for electron transport, represents computational result in the case when boundary conditions (18) and (19) for the electron number density and energy density at the cathode are replaced with following:

$$\hat{\mathbf{n}} \cdot \mathbf{\Gamma}_e = 1/2 v_e n_e - \gamma \hat{\mathbf{n}} \cdot \mathbf{\Gamma}_i, \tag{23}$$

$$\hat{\mathbf{n}} \cdot \mathbf{\Gamma}_\varepsilon = 5/6 v_e n_\varepsilon - \bar{\varepsilon}\gamma \hat{\mathbf{n}} \cdot \mathbf{\Gamma}_i. \tag{24}$$

These boundary conditions are default boundary conditions for the electron transport in the dc glow discharge model

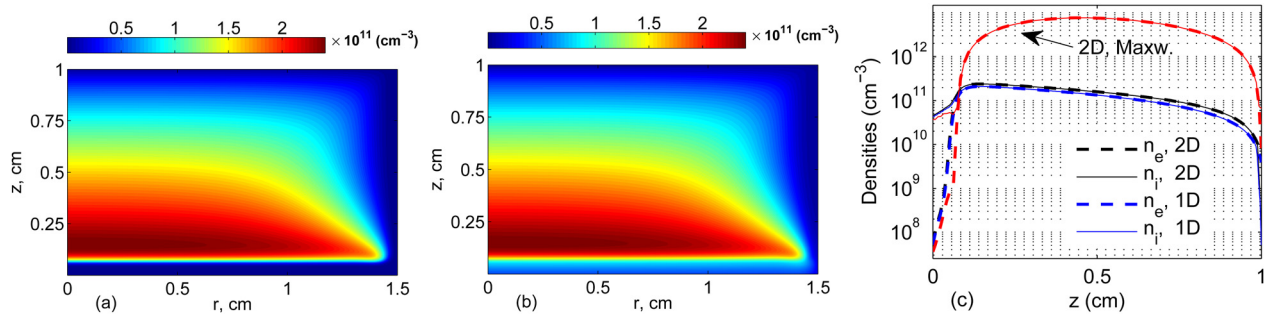

FIG. 6. (Color online) The same as in Fig. 4 but for the regime 7 in the Fig. 3 and Table II.

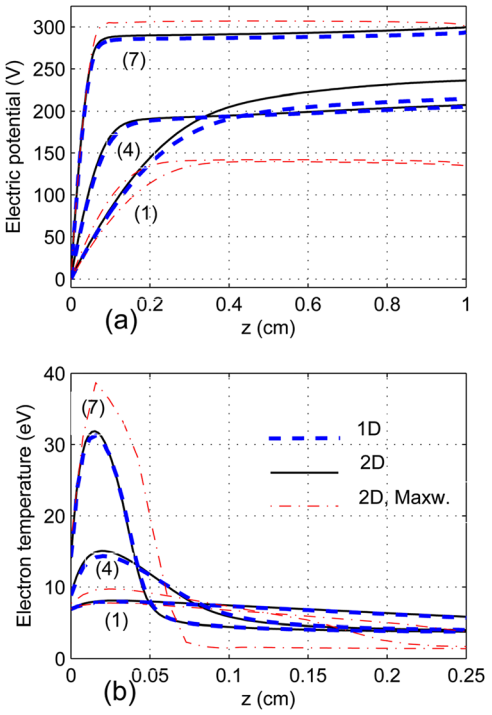

FIG. 7. (Color online) Axial profiles of (a) electric potential, ϕ, and (b) electron temperature, T_e, for the regimes 1, 4, and 7 in the Fig. 3 and Table II. Dotted lines: 1D solution, solid lines: 2D solution. 'Maxw' indicates result with the Maxwellian EEDF.

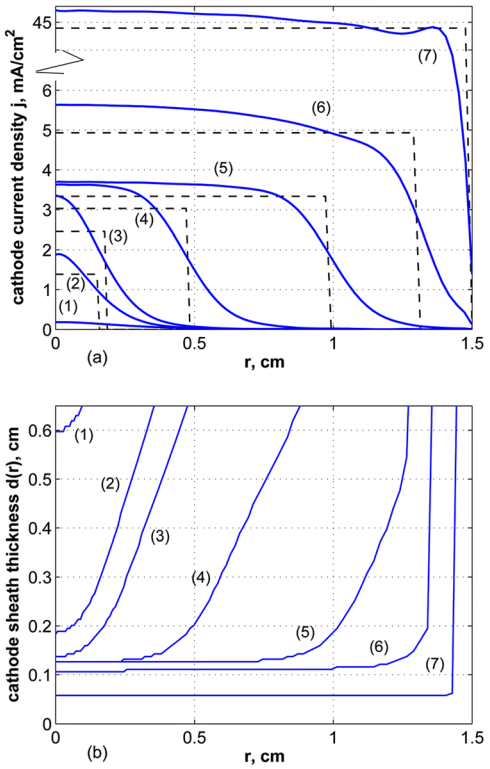

FIG. 8. (Color online) (a) Cathode current density and (b) cathode sheath thickness radial profiles for the parameter regimes 1–7 from Fig. 3.

from the COMSOLs Model Library.[23] Here, ion flux density $\mathbf{\Gamma}_i$ is specified at the boundary as $[\alpha\mu_i(\hat{\mathbf{n}}\cdot\mathbf{E})n_i + 1/2v_i n_i]$, and for mean energy of electrons emitted by incidence of ions, we used $\bar{\varepsilon} = 3/2k_B T_e$.[23]

It should be clarified that numerical results presented in Figs. 4–14 (excepting Fig. 9 which compares different model solutions) have been obtained by the model called "comsol, b-in" above.

Calculations showed that the numerical results obtained from the "equation based" COMSOL model and those from the built-in Plasma Module coincide almost exactly in 1D. Although the agreement in 2D is not perfect (compare "comsol e-b" and "comsol, b-in 2" curves in Fig. 3(a)), model solutions tends to converge to each other with the computational grid refinement.

We also carried out the comparison of COMSOL and CFD-ACE+ calculation results (employing the same transport coefficients and plasma chemistry), which are found to be in good agreement. CVC of the discharge obtained from CFD-ACE+ is line labelled by "cfd-ace+" in the Fig. 3(a).

Figure 9 compares the spatial profiles of 1D discharge parameters for the conditions Ref. 11 (namely, for $p = 1$ torr argon, applied voltage $U_d = 250$ V, discharge gap $L = 1$ cm, and $\gamma = 0.06$), obtained by COMSOL models, CFD-ACE+ solver, and Becker *et al.*[22]

Notice that for the "equation based" and with built-in Plasma Module COMSOL models, profiles of electric field (Fig. 9(b), lines "comsol e-b" and "comsol, bi-n 1") and mean electron energy (Fig. 9(c)) practically coincide, agreement between the number density profiles is not perfect, but the difference tends to decrease with computational grid refinement.

Fig. 9 show that there is a discrepancy with the numerical results of the "extended fluid model" described in Ref. 22, which is caused by the different transport parameters and plasma chemistry, employed in that study. However, note that the absolute magnitudes of the discharge plasma parameters are in good agreement with COMSOL results subject to conditions (23) and (24), but cathode sheath thicknesses predicted by the calculations and consequently the discharge currents are different.

In regard to comparison with the CFD-ACE+ solver results, while the electric field and mean electron energy profiles are in good agreement (Figs. 9(b) and 9(c)), the difference in the density profiles is more pronounced (Fig. 9(a)), and, surprisingly, this difference (as well as the difference in CVC curves derived from the COMSOL and CFD-ACE+ based models, which can be observed in the Fig. 3(a)) does not tend to disappear with grid refinement in the employed models. The analysis carried out shows that the difference in COMSOL and CFD-ACE+ modelling results might be caused by the difference in the boundary conditions actually imposed for n_e and n_ε in CFD-ACE+ solver from those declared in Ref. 27, which are our conditions (16)–(19).

Figs. 3–7 also demonstrate the numerical result in the case of Maxwellian EEDF. Fig. 3(a) shows how the CVC curve changes considerably in this case. The axial distributions of electron and ion number densities are shown in panels (c) of Figs. 4–6, and the electric potential and electron temperature in Fig. 7. Although the parameter regimes have been taken to produce the same discharge currents as for the corresponding discharge with EEDF calculated from the Boltzmann equation, notice that magnitudes of discharge characteristics differ significantly.

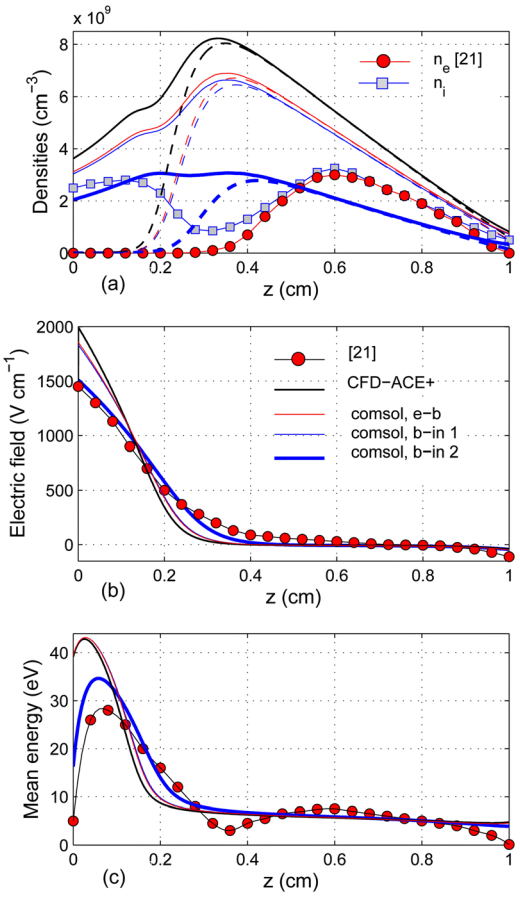

FIG. 9. (Color online) 1D calculation results for $p = 1$ torr, $U_d = 250$ V, $L = 1$ cm, and $\gamma = 0.06$. (a) Ion (solid line) and electron (dash line) number densities, n_i and n_e, (b) electric field E, and (c) mean electron energy $\bar{\varepsilon}$. Lines with markers: data from Refs. 22 and 11.

We also compared CPU and memory requirements for COMSOL MULTIPHYSICS and CFD-ACE+ for a typical 2D discharge conditions (point 7 in Fig. 3(a)). Calculations were performed on a PC with Intel Core i7 2600 (4 CPU@ 3.4 GHz, 8 threads, 16 GB RAM). We used orthogonal grids, containing 60×50, 120×100, and 240×200 cells. Time step was taken constant equal to $\Delta\tau = 5 \times 10^{-9}$ s. Simulations were started from the same initial condition, and continued for 22 440 steps $\Delta\tau$, which cover a time interval of 0.112 ms, such that a steady state is almost reached. Meaningful information on performance of these solvers can be gained from the average time lengths spent for one step $\Delta\tau$. For the grids described above, these are 0.41 s, 1.43 s, and 6.23 s in the case of COMSOL, and noticeably greater in the case of CFD-ACE+, namely, 0.51 s, 2.33 s, and 10 s. However, memory required by COMSOL (1.6, 2.0, and 2.9 GB) is about one order in magnitude greater than that of CFD-ACE+ (21.7, 38.6, and 90 MB).

It should be emphasized that COMSOL MULTIPHYSICS, as opposed to CFD-ACE+, which is a fixed time step solver, can run with a variable time step that significantly reduces time consumption. To be more specific, COMSOL simulation of the problem above but with a variable time step leads to about fifty-fold decrease in execution time and takes 3.1, 10.2, and 44.7 minutes on the grid with 60×50, 120×100, and 240×200 cells, while with a fixed $\Delta\tau = 5 \times 10^{-9}$ s, the total time consumed is large as 2.5, 8.9, and 38.8 hours correspondingly.

It should be also noted that numerical values above are given for demonstration of a general tendency. Actual performance of COMSOL and CFD-ACE+ (which are two rather different software packages, employing different numerics, where first is based on finite element analysis, while second on the finite volume method) can be affected by a number of parameters and settings for nonlinear method and linear solvers, and tolerances.

B. Comparison of 1D and 2D modelling results

A significant part of numerical studies of glow discharges is limited to one-dimensional geometry. The reason is that one-dimensional (1D) modelling strongly reduces the computational cost that is especially important in the case of kinetic and hybrid approaches employing detailed plasma chemistry models. However, it is obvious that accuracy of 1D model predictions, in general, is of limited usefulness. Here, as a certain test of applicability of 1D approximation, we perform comparison of 1D and 2D modelling results for the discharge conditions considered in the previous sections.

Figure 3(b) shows CVC curves for the 1D and 2D discharge models (argon at pressure $p = 3$ torr, $L = 1$ cm, and $R = 1.5$ cm) in $U_d = U_d(J_d)$ coordinates, where U_d denotes the voltage and J_d the current density. Note that CVC for 1D discharge has the form $U_d = U_d(J_d)$ by itself. However, in the 2D case, current density J_d was calculated as an average current through the cathode spot, with the spot radius being

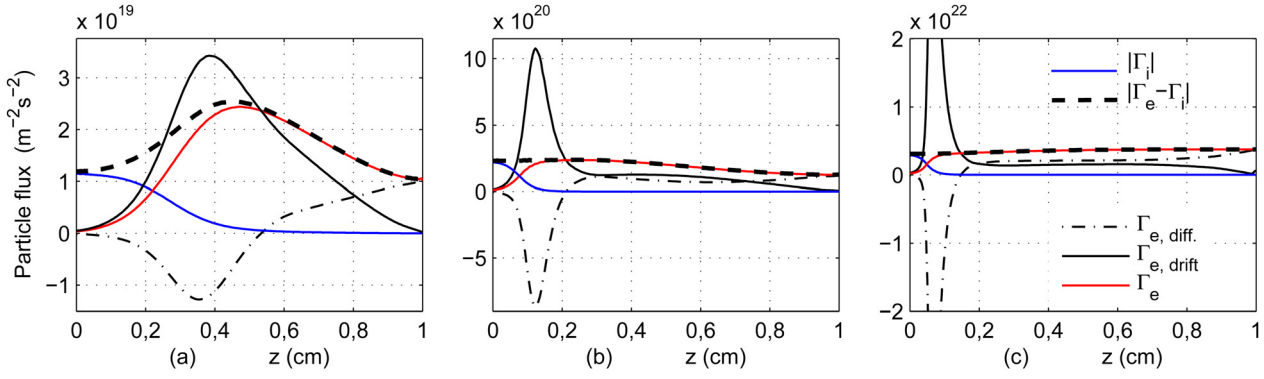

FIG. 10. (Color online) Axial profiles of axial components of ion flux, $\mathbf{\Gamma}_i$, and drift, diffusion, and total electron fluxes, $\mathbf{\Gamma}_{e,drift}$, $\mathbf{\Gamma}_{e,diff}$, and $\mathbf{\Gamma}_e$, and difference $\mathbf{\Gamma}_e - \mathbf{\Gamma}_i$. Panels (a), (b), and (c) correspond to the parameter regimes 1, 4, and 7 in Fig. 3.

the distance from the symmetry axis where the current density reduces by one half. (These current density magnitudes are indicted by the horizontal profiles in the Fig. 8(a), and also listed in the Table II.) Values of the normal cathode layer thickness $pd = 0.39$ Torr · cm and normal current density $J_d/p^2 = 0.34$ mA/(cm^2 Torr^2) agrees well with the published data (see, e.g., Ref. 1, pp 182–183 and Ref. 28).

Let us now consider longitudinal distributions of the 1D and 2D discharge parameters, for the same three parameter regimes, considered in previous sections, namely, the regimes indicated by the numbers 1, 4, and 7 in the Fig. 3 and Table II (the current magnitudes for theses regimes are $I_d = 8.8 \times 10^{-5}$ A, 2.9×10^{-3} A, and 0.31 A). In order to observe similar discharge regimes in 1D and 2D, conditions for the 1D discharges were chosen to produce current density, fitting the mean current density (over the cathode spot) of the corresponding two-dimensional discharges.

Panels (c) in the Figs. 4, 5, and 6 and Fig. 7(a) compare the axial profiles of the electron and ion number densities, n_e and n_i, in subnormal, normal, and abnormal discharge, for 1D and 2D models. Axial profiles of the electric potential, ϕ, and the electron temperature, T_e, obtained within the 2D model are shown in Figs. 7(b) and 7(c).

As can be seen from these figures, for the present discharge conditions with $L < R$, the one-dimensional model describes well the glow discharge properties, especially in the case of abnormal discharge (note that abnormal branches of CVC curves for 1D and 2D models spaced closely enough together in the Fig. 3(b)), which spatial profiles are essentially "one-dimensional." This agreement between 1D and 2D modelling results is supported by the analysis in Ref. 20, according with which the 1D approximation for the glow discharge models is applicable in the case where the discharge's transverse dimension far exceeds its longitudinal dimension (the discharge radius R is greater than the discharge gap L) and discharge occupies the cathode surface entirely. This agreement is disrupted in the normal regime, because of the 2D effects (such as formation of the normal current density and discharge contraction) which can not be reproduced within the 1D approximation.

IV. PARTICLE FLUX PROFILES

Figures 10–12 demonstrate axial and radial profiles of particle fluxes in the discharge, for the typical three regimes, namely, for the abnormal, normal, and subnormal modes, which correspond to the points 7, 4, and 1 in the CVC curve in Fig. 3. Axial profiles of the electron drift, $\mathbf{\Gamma}_{e,drift} = -n_e \mu_e \mathbf{E}$, diffusion, $\mathbf{\Gamma}_{e,diff} = -D_e \nabla n_e$, and of the total flux, $\mathbf{\Gamma}_e = -n_e \mu_e \mathbf{E} - D_e \nabla n_e$, as well as the axial profiles of the total ion flux $\mathbf{\Gamma}_i = n_i \mu_i \mathbf{E} - D_i \nabla n_i$, and the difference of electron and ion fluxes (which is proportional to the current density) are shown in Fig. 10. Radial profiles (along the discharge chamber midsection, i.e., the line $z = 0.5$ cm) of the total electron and ion fluxes $\mathbf{\Gamma}_e$ and $\mathbf{\Gamma}_i$ as well as their difference $\mathbf{\Gamma}_e - \mathbf{\Gamma}_i$ is presented in Fig. 11. It can be seen that $\mathbf{\Gamma}_e \gg \mathbf{\Gamma}_i$ throughout the discharge cross section for the regimes 7 and 4 (panels (a) and (b)), where the plasma is essentially quasineutral. Finally, Fig. 12 plots the drift and diffusion components of electron flux $\mathbf{\Gamma}_{e,drift}$ and $\mathbf{\Gamma}_{e,diff}$ from Fig. 11, which demonstrate the fact that the total electron flux is about one order of magnitude smaller compared to its drift and diffusion components.

Analysis performed in Ref. 25 has shown that the multi-dimensional geometry leads to the emergence of vortex electric currents in plasmas even in the absence of the magnetic field. Although the theoretical analysis in Ref. 25 has been carried out for a different discharge configuration, namely, for the ICP discharge bounded by dielectric walls, it has been stated that occurrence of vortex current in multi-dimensional plasmas is the rule and its absence the exception. The theoretical analysis of the electric discharges where the currents flow through the walls, specifically the dc discharges, are much more complicated. However, numerical calculations in cylindrical 2D geometry reveal that the vortex component of the electric current occurs in the dc glow discharges just as it do in the case of "current free" plasmas. More precisely, the reduced current density $\tilde{\mathbf{J}} = \mathbf{J} - \mathbf{J}_0$, obtained by subtracting the constant vector $\mathbf{J}_0 = (0, \bar{J})$, where $\bar{J} = \left(2\pi \int_0^R J_z(r,z) r dr\right)/(\pi R^2)$ denotes the averaged (over the cathode surface) current density, from the discharge current density $\mathbf{J} = (J_r, J_z)$, forms the vector field, where current streamlines are closed (see Fig. 13, which illustrates the result for the same modes as in previous sections, corresponding to regimes "1," "4," and "7" in the CVC curve (Fig. 3)). Since $\nabla \times \mathbf{J} = \nabla \times \tilde{\mathbf{J}}$, this means that the discharge current density $\mathbf{J}$ also has the vortex nature.

For the axially symmetric dc discharges, the vortex feature of the current density leads to distinction in the radial

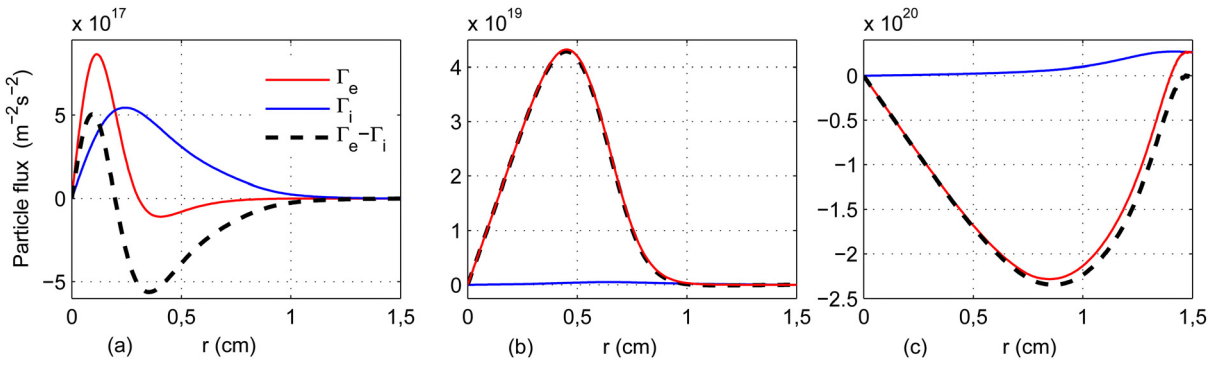

FIG. 11. (Color online) Radial profiles of radial components of ion and electron fluxes $\mathbf{\Gamma}_i$ and $\mathbf{\Gamma}_e$ and their difference $\mathbf{\Gamma}_e - \mathbf{\Gamma}_i$. Panels (a), (b), and (c) correspond to parameter regimes 1, 4, and 7 in Fig. 3.

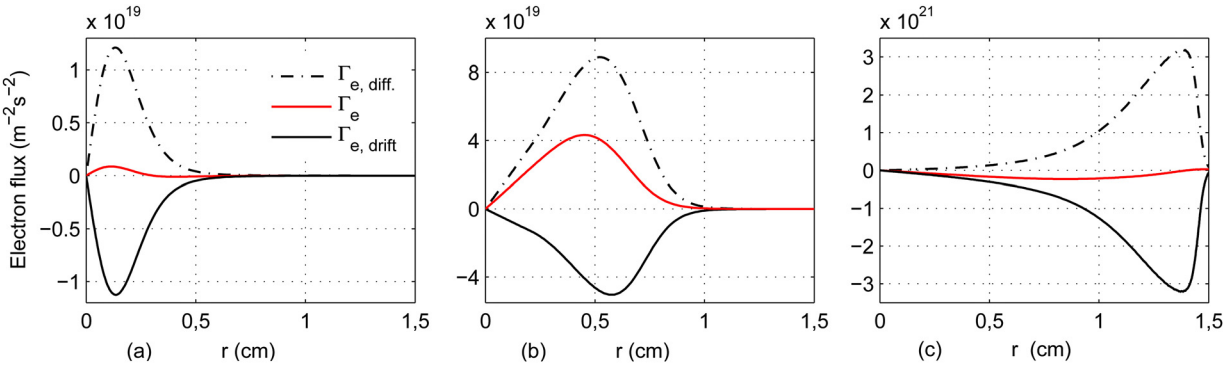

FIG. 12. (Color online) Radial profiles of radial components of the drift, diffusion, and total electron fluxes, $\mathbf{\Gamma}_{e,drift}$, $\mathbf{\Gamma}_{e,diff}$, and $\mathbf{\Gamma}_e$. Panels (a), (b), and (c) correspond to parameter regimes 1, 4, and 7 in Fig. 3.

components of the electron and ion fluxes. In fact, radial components of vectors $\mathbf{J}$ and $\widetilde{\mathbf{J}}$ coincide, and reduced electric current density $\widetilde{\mathbf{J}}$ is a vector field having closed streamlines. Consequently, for certain value of axial coordinate z, radial profile $\widetilde{J}_r(r,z)$ is different from zero and thus the radial profile $J_r(r,z)$ for this coordinate z is also different from zero. Since

$$\mathbf{J} = e(\mathbf{\Gamma}_i - \mathbf{\Gamma}_e), \tag{25}$$

inequality $J_r \neq 0$ implies the difference in the radial components of the electron and ion fluxes, which means that the commonly accepted *ambipolarity* condition

$$\mathbf{\Gamma}_e = \mathbf{\Gamma}_i \tag{26}$$

is violated for the radial fluxes of charged particles. Radial profiles of radial components of electron flux and ion flux and their difference, which is proportional to the radial component of the electric current density, are shown in Fig. 11. As can be seen from these figures, the electron and ion fluxes coincide on the dielectric wall, where consequently the current density vanishes (since it cannot flow through the dielectric).

Figure 14 demonstrates the calculation results in the case of longer dc discharge (with gap $L = 5$ cm and tube radius $R = 0.5$ cm) having the positive column region. In the positive column, all the plasma parameters are functions of the radial coordinate r only. Therefore, continuity equation for the current density

$$\nabla \cdot \mathbf{J} = 0 \tag{27}$$

takes the form

$$\frac{1}{r}\frac{\partial}{\partial r}(rJ_r) = 0, \tag{28}$$

from which

$$rJ_r = Const. \tag{29}$$

Since current density has to vanish on the dielectric wall, $J_r(r = R) = 0$, the constant in the right-hand side of Eq. (29) must be zero, and therefore, in the positive column region, as suggested by Eq. (25), radial components of the electron and ion fluxes coincide,

$$\mathbf{\Gamma}_{e,r} = \mathbf{\Gamma}_{i,r}. \tag{30}$$

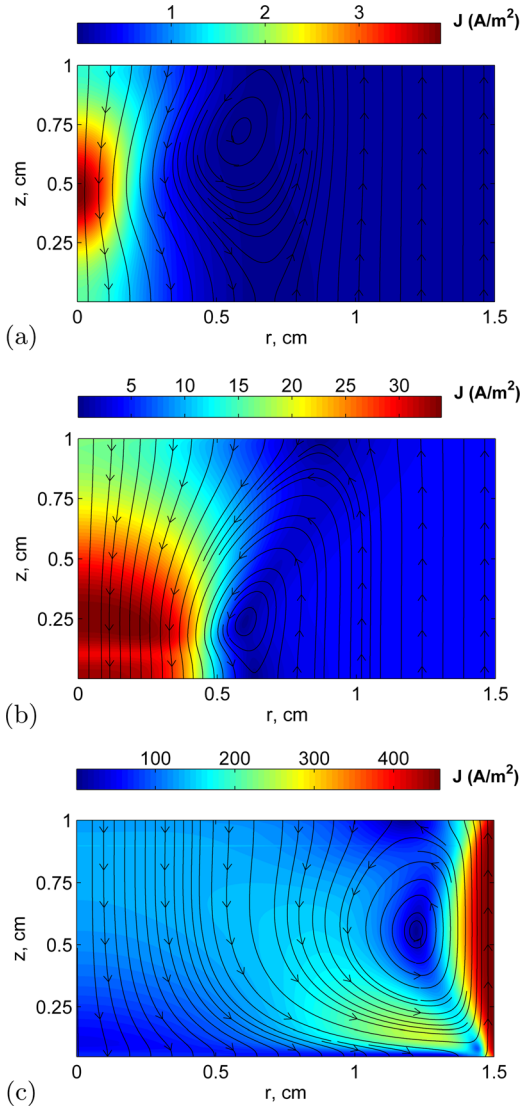

FIG. 13. (Color online) 2D distribution of magnitude of the reduced current density and streamlines of the reduced current density $\widetilde{\mathbf{J}} = (J_r, J_z - \bar{J})$, for parameter regime (a) 1, (b) 4, and (c) 7 from Fig. 3.

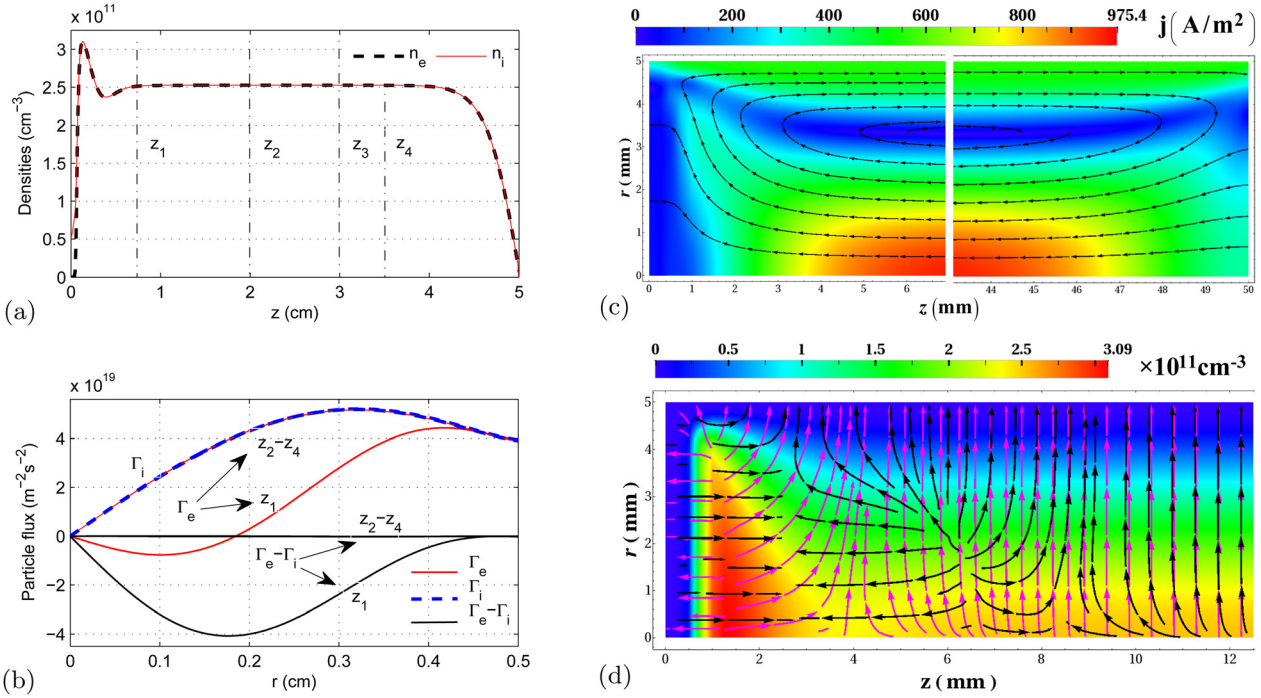

FIG. 14. (Color online) (a) Axial profiles of electron and ion number densities, n_e and n_i. (b) Radial profiles of radial components of ion and electron fluxes, $\mathbf{\Gamma}_i$ and $\mathbf{\Gamma}_e$, and their difference, $\mathbf{\Gamma}_e - \mathbf{\Gamma}_i$, over the cross sections through the points indicated on the panel (a). (c) 2D distribution of magnitude of the reduced current density and streamlines of the reduced current density (anode and cathode regions shown). (d) 2D distribution of electron density, n_e, and streamlines of ∇T_e and ∇n_e (cathode region shown). Pressure $p = 3$ torr, $U_d = 480$ V, $L = 5$ cm, $R = 0.5$ cm, $\gamma = 0.1$.

This is illustrated in Fig. 14(b), which shows the radial profiles of the ion and electron flux densities, $\mathbf{\Gamma}_i$ and $\mathbf{\Gamma}_e$, and their difference, over the cross sections through the points $z = 0.75$, 2, 3, and 3.5 cm indicated in Fig. 14(a). Notice that electron and ion radial fluxes coincide perfectly for points $z = 2$, 3, and 3.5 cm, which locate in the positive column, where, therefore, the radial particle flux is pure ambipolar.

Condition for emergence of vortex electric currents, namely, $\nabla T_e \times \nabla n \neq 0$, which is equivalent to the condition that vectors ∇n and ∇T_e are not parallel, derived in Ref. 25 for the ICP discharge with dielectric walls, can be generalized to the case of dc discharges. (In this condition, $n = n_e \approx n_i$ denotes the common number density.) More specifically, nonuniformity of electron transport coefficients leads to development of vortex currents in dc discharge plasma, and hence, conditions $\nabla \times \mathbf{J} \neq 0$ is satisfied.

Since

$$\begin{aligned}\mathbf{J} &= e(\mathbf{\Gamma}_i - \mathbf{\Gamma}_e)\\ &= -e[-(D_e - D_i)\nabla n + (\mu_e + \mu_i)\nabla\phi],\end{aligned} \tag{31}$$

and equalities $\nabla \times \nabla u = 0$ and $\nabla \times (u\nabla v) = (\nabla u) \times (\nabla v)$ hold for arbitrary scalars u and v, curl of $\mathbf{J}$ has the following form,

$$\begin{aligned}\nabla \times \mathbf{J} = e\frac{\mathrm{d}D_e(T_e)}{\mathrm{d}T_e}\nabla T_e \times \nabla n - en\frac{\mathrm{d}\mu_e(T_e)}{\mathrm{d}T_e}\nabla T_e \times \nabla\phi\\ - e(\mu_e + \mu_i)\nabla n \times \nabla\phi.\end{aligned} \tag{32}$$

Further from the Boltzmann distribution for electrons, it follows that

$$\phi = T_e \ln(n/n_0), \tag{33}$$

and hence

$$\nabla\phi = \frac{\phi}{T_e}\nabla T_e + \frac{T_e}{n}\nabla n. \tag{34}$$

Substituting $\nabla\phi$ from the last equation in (32), we obtain

$$\nabla \times \mathbf{J} = e\left[\frac{\mathrm{d}D_e(T_e)}{\mathrm{d}T_e} - T_e\frac{\mathrm{d}\mu_e(T_e)}{\mathrm{d}T_e} + \frac{(\mu_e + \mu_i)\phi}{T_e}\right]\nabla T_e \times \nabla n. \tag{35}$$

Since factor in square brackets in (35), in general, is different from zero, then $\nabla \times \mathbf{J} = 0$ iff $\nabla T_e \times \nabla n = 0$. Moreover, since profiles of n and T_e are determined by different balance equations, their gradients ∇T_e and ∇n, in general, are not parallel, $\nabla T_e \times \nabla n \neq 0$, and hence in dc discharges $\nabla \times \mathbf{J} \neq 0$ and current density vector has a vortex structure. This is confirmed by the calculation results illustrated in Fig. 14(d), which plots the streamlines of ∇T_e (red lines) and ∇n_e (black lines).

V. CONCLUSIONS

Since nonequilibrium kinetic processes, in principle, cannot be treated within the framework of a fluid model, any correct description of the glow discharge requires kinetic analysis of the electron behavior. Here, we studied and tested the so called "extended fluid model" for a glow discharge. The idea of the "extended fluid model" represents a certain compromise between strictly fluid and kinetic models. This

approach employs a fluid description for heavy (charged and neutral) particles and a more rigorous kinetic description of electron dynamics: electron transport (diffusion coefficient and mobility) as well as the rates of electron-induced plasma-chemical reactions are calculated using the Boltzmann equation for electron energy distribution function and corresponding collision cross-sections. The self-consistent electric field was calculated using the Poisson equation.

We used COMSOL MULTIPHYSICS software for modelling and numerical solutions. We implemented two modelling approaches. First, we derived the model from the COMSOL pde's and, second, using built-in COMSOL's Plasma Module with DC Discharge interface.

Calculations (for a low pressure argon gas) showed that these COMSOL models lead to essentially identical results, which converge to each other with computational grid refinement, and agree well with the CFD-ACE+ solver result.

Analysis of the calculation results showed that this model describes adequately most of the fundamental properties of the glow discharge, reproduces correctly current-voltage characteristics (CVC) and specific discharge modes occurring along the CVC, as well as the two-dimensional spatial profiles of the discharge parameters (such as the charged particle densities, temperature, and the electric potential and field).

We also analyzed the spatial distributions of particles fluxes in plasma of short and longer glow discharges. Numerical calculations confirm previously reported results[25] that in multidimensional plasmas, vortex electric currents occur even in the absence of magnetic field. These vortex currents reveal themselves, in particular, in violation of the ambipolarity condition for radial components of electron and ion fluxes for shorter glow discharge. However, in the positive column region of longer discharge, since all the discharge parameters there depend on the radial coordinate only, the geometry becomes one-dimensional, and therefore, the condition of ambipolarity of fluxes is satisfied.

ACKNOWLEDGMENTS

The work was supported by the joint research grant from the Scientific and Technical Research Council of Turkey (TUBITAK) 108T586 and Russian Foundation for Basic Research (RFBR).

[1]Yu. P. Raizer, *Gas Discharge Physics* (Springer-Verlag, Berlin, 1991).
[2]V. I. Kolobov and L. D. Tsendin, Phys. Rev. A **46**, 7837 (1992).
[3]A. A. Kudryavtsev, A. V. Morin, and L. D. Tsendin, Tech. Phys. **53**, 1029 (2004).
[4]R. Winkler, S. Arndt, D. Loffhangen, F. Sigeneger, and D. Uhrlandt, Contrib. Plasma Phys. **44**, 437 (2004).
[5]V. Kolobov and R. Arslanbekov, IEEE Trans. Plasma Sci. **34**, 895 (2006).
[6]R. E. Robson, R. D. White, and Z. Lj, Petrovich, Rev. Mod. Phys. **77**, 1303 (2005).
[7]R. D. White, R. E. Robson, S. Dujko, P. Nicoletopoulos, and B. Li, J. Phys. D: Appl. Phys. **42**, 194001 (2009).
[8]A. Fiala, L. C. Pitchford, and L. C. Boeuf, Phys. Rev. E **49**, 5607 (1994).
[9]M. J. Kushner, J. Phys. D: Appl. Phys. **42**, 194013 (2009).
[10]M. Surenda, D. B. Graves, and G. M. Jellum, Phys. Rev. A **41**, 1112 (1990).
[11]A. Derzsi, A. Hartmann, I. Korolov, J. Karacsony, G. Bano, and Z. Donko, J. Phys. D: Appl. Phys. **42**, 225204 (2009).
[12]Z. Donko, P. Hartmann, and K. Kutasi, Plasma Sources Sci. Technol. **15**, 178 (2006).
[13]J. Dijk, G. M. W. Kroesen, and A. Bogaerts, J. Phys. D: Appl. Phys. **42**, 190301 (2009).
[14]J. P. Boeuf, Phys. Rev. A **36**, 2782 (1987).
[15]J. P. Boeuf and L. C. Pitchford, Phys. Rev. E **51**, 1376 (1995).
[16]R. Arslanbekov and V. Kolobov, J. Phys. D: Appl. Phys. **36**, 2986 (2003).
[17]G. K. Grubert, M. M. Becker, and D. Loffhagen, Phys. Rev. E **80**, 036405 (2009).
[18]G. J. M. Hagelaar and L. C. Pitchford, Plasma Sources Sci. Technol. **14**, 722 (2005).
[19]Y. Sakiyama, D. V. Graves, and E. Stoffels, J. Phys. D: Appl. Phys. **41**, 095204 (2008).
[20]E. A. Bogdanov, S. F. Adams, V. I. Demidov, A. A. Kudryavtsev, and J. M. Williamson, Phys. Plasmas **17**, 103502 (2010).
[21]E. A. Bogdanov, K. D. Kapustin, A. A. Kudryavtsev, and A. S. Chirtsov, Tech. Phys. **55**, 1430 (2010).
[22]M. M. Becker, D. Loffhagen, and V. Schmidt, Comput. Phys. Commun. **180**, 230 (2009).
[23]COMSOL MULTIPHYSICS™ 4.1 (2010), COMSOL Inc., http://www.comsol.com
[24]CFD-ACE+™ (2003), CFD Research Corporation, http://www.cfdrc.com/
[25]E. A. Bogdanov, A. S. Chirtsov, and A. A. Kudryavtsev, Phys. Rev. Lett. **106**, 195001 (2011).
[26]G. J. M. Hagelaar, F. J. Hoog, and G. M. W. Kroesen, Phys. Rev. E **62**, 1452 (2000).
[27]CFD-ACE+™ V2004, *Modules Manual* (ESI US R&D Inc., 2004), Vol. 2, pp. 135–136.
[28]A. V. Phelps, Plasma Sources Sci. Technol. **10**, 180 (2001).